

SCJD: Sparse Correlation and Joint Distillation for Efficient 3D Human Pose Estimation

1st Weihong Chen

South China University of Technology
cswilliam@mail.scut.edu.cn

2nd Xuemiao Xu*

South China University of Technology
xuemx@scut.edu.cn

3rd Haoxin Yang*

South China University of Technology
harxis@outlook.com

4th Yi Xie

South China University of Technology
yixie@stu.hqu.edu.cn

5th Peng Xiao

South China University of Technology
Polarispro.xiao@gmail.com

6th Cheng Xu

The Hong Kong Polytechnic University
cschengxu@gmail.com

7th Huaidong Zhang

South China University of Technology
huaidongz@scut.edu.cn

8th Pheng-Ann Heng

The Chinese University of Hong Kong
pheng@cse.cuhk.edu.hk

Abstract—Existing 3D Human Pose Estimation (HPE) methods achieve high accuracy but suffer from computational overhead and slow inference, while knowledge distillation methods fail to address spatial relationships between joints and temporal correlations in multi-frame inputs. In this paper, we propose *Sparse Correlation and Joint Distillation* (SCJD), a novel framework that balances efficiency and accuracy for 3D HPE. SCJD introduces *Sparse Correlation Input Sequence Downsampling* to reduce redundancy in student network inputs while preserving inter-frame correlations. For effective knowledge transfer, we propose *Dynamic Joint Spatial Attention Distillation*, which includes *Dynamic Joint Embedding Distillation* to enhance the student’s feature representation using the teacher’s multi-frame context feature, and *Adjacent Joint Attention Distillation* to improve the student network’s focus on adjacent joint relationships for better spatial understanding. Additionally, *Temporal Consistency Distillation* aligns the temporal correlations between teacher and student networks through upsampling and global supervision. Extensive experiments demonstrate that SCJD achieves state-of-the-art performance. Code is available at <https://github.com/wileychan/SCJD>.

Index Terms—3D human pose estimation, knowledge distillation.

I. INTRODUCTION

3D Human Pose Estimation (HPE) detects 3D joint coordinates from monocular video and is widely used in downstream tasks like action recognition [1], [2] and motion analysis [3], [4]. To achieve high accuracy, prior methods typically use multi-frame input sequences to capture temporal dependencies [5]–[12] and large networks (e.g., Vision Transformers [13]) for feature extraction. However, these approaches are computationally expensive and suffer from slow inference speeds due to dense inputs and significant network overhead.

To balance 3D HPE computational efficiency and accuracy, recent studies have adopted strided convolutions [14]

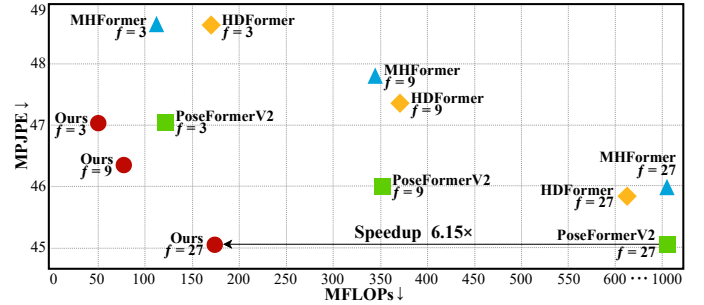


Fig. 1. Comparison between the previous methods PoseFormerV2 [15], HDFormer [8], MHFormer [10] and our SCJD on Human3.6M. f represents the length of the input sequence. For both metrics, the smaller Mean Per Joint Position Error (MPJPE) and floating-point operations (FLOPs), the better.

or frequency-domain features [15], [16] to avoid processing long input sequences. However, these approaches require deeper and wider networks to sustain accuracy, still resulting in significant computational demands. Knowledge distillation (KD) [17] has also been explored to address this challenge [18]–[20]. These methods train a light student network to replicate the output logits [18] or the final-layer features [19], [20] of heavy teacher network. Despite their potential, these methods are limited by their reliance on single-image inputs, neglecting the temporal correlations between actions in consecutive frames—an essential factor in resolving the 2D-to-3D ambiguity in monocular HPE. Furthermore, these approaches fail to emphasize that the student network should prioritize learning the relationships between human joints from the teacher network rather than merely replicating final outputs or high-level semantic features. These limitations ultimately restrict their accuracy and performance.

To address these challenges, we propose a novel *Sparse Correlation and Joint Distillation* (SCJD) for 3D HPE. Our key insight is to leverage sparse input sequences and KD to

reduce computational overhead while maintaining accuracy. Specifically, Our approach begins with *Sparse Correlation Input Sequence Downsampling*, which sparsifies the student network’s inputs to reduce redundancy while preserving inter-frame correlations more effectively than single-frame methods. Next, to transfer knowledge effectively from a dense, heavy teacher network to a sparse, lightweight student network, we introduce *Dynamic Joint Spatial Attention Distillation*, which comprises two components: a) *Dynamic Joint Embedding Distillation*, which aggregates the local context information of teacher’s spatial encoder to enhance the student’s spatial feature representation. b) *Adjacent Joint Attention Distillation*, which employs an adjacent joint attention matrix to guide the student network in focusing on connections between adjacent joints, improving its understanding of human posture. Finally, we propose *Temporal Consistency Distillation*, which aligns the temporal correlation between input contexts by upsampling the student’s features to match the teacher network’s outputs, and complemented by global supervised learning with ground truth. Our extensive experiments validate our method’s superiority over existing state-of-the-art techniques in terms of both efficiency and accuracy.

To summarize, our contributions are threefold:

- We propose a novel framework SCJD, which enhances the efficiency and accuracy of 3D HPE by utilizing sparse correlation inputs and dynamic joint spatial attention distillation.
- We introduce dynamic joint embedding distillation and adjacent joint attention distillation, enabling better alignment of joint spatial features between the teacher and student spatial encoder, significantly improving the student model’s performance.
- Extensive experiments demonstrate that our method achieves superior speed-accuracy trade-offs, delivering up to $6.15\times$ speedup with comparable accuracy, as illustrated in Fig. 1.

II. RELATED WORK

A. Efficient 3D Human Pose Estimation

The goal of efficient 3D human pose estimation is to strike a balance between accuracy and computational efficiency. While recent studies [5]–[11] have prioritized improving accuracy, fewer have tackled the challenge of computational efficiency. Early efficient methods, such as Choi et al. [21], achieved faster pose estimation by utilizing compact networks and skip concatenation to reduce computational complexity. However, these approaches rely on single-frame inputs, which lack temporal context and limit accuracy compared to more advanced methods. Multi-frame inputs improve accuracy but increase computational demands. To address this, Li et al. [14] used strided convolutions to reduce the sequence length while capturing local context. Zhao et al. [15] encoded longer sequences into low-frequency coefficients combined with shorter pose sequences. While these methods reduce input length, they still require deeper, wider networks, leading to higher computational costs.

B. Knowledge Distillation in 3D Human Pose Estimation

Knowledge distillation [17] is an effective technique for compressing networks by transferring knowledge from a large teacher network to a lightweight student network using deep learning technology [22], [23], improving the latter’s accuracy. Several studies [18]–[20], [24], [25] have applied distillation to accelerate 3D human pose estimation. Hwang et al. [18] trained a student network to mimic the teacher’s output logits, while Kim et al. [19] used pruning and feature imitation to boost performance. Bian et al. [20] transferred multi-view stereo knowledge to the student model. However, these methods are limited to single-frame inputs and fail to utilize multi-frame video context, which is crucial for resolving 2D-to-3D ambiguities. Additionally, they overlook the importance of teaching the student network to learn joint spatial relationships. Our approach addresses these gaps by designing a distillation framework that incorporates multi-frame context while emphasizing joint relationships.

III. PROPOSED METHOD

A. Overview

To maintain 3D HPE performance while maximizing computational efficiency, we propose SCJD, a framework that seamlessly integrates sparse correlation inputs and dynamic joint distillation for efficient and accurate 3D HPE. The detailed network architecture is illustrated in Fig. 2(a). Building on PoseFormer [26], we introduce *Sparse Correlation Input Sequence Downsampling* to reduce input redundancy while preserving temporal correlations. Additionally, we employ *Dynamic Joint Embedding Distillation*, *Adjacent Joint Attention Distillation*, and *Temporal Consistency Distillation* to transfer knowledge from the teacher network to a lightweight student model. This approach enables the network to efficiently process a 2D pose input sequence $X \in \mathbb{R}^{f \times (J \cdot 2)}$ of f frames, where J represents the number of joints, and accurately predict the 3D pose $y \in \mathbb{R}^{1 \times (J \cdot 3)}$ for the center frame of the sequence.

B. Sparse Correlation Input Sequence Downsampling

To minimize redundant information across video frames, we propose leveraging sparse inputs to expand the receptive field, enhancing both model accuracy and efficiency. Unlike the teacher network, which uses continuous 2D pose sequences, our lightweight student network employs *sparse correlation input sequences* through strategic sampling. As illustrated in Fig. 2(b), for a 2D pose sequence of length f^T in the teacher network, the student network samples equidistantly both forward and backward from the center frame using a stride L , ensuring alignment between the student and teacher networks at the center frame. This sampling reduces the student network’s input sequence length to $f^S = f^T / L$. For example, if the teacher network processes a sequence of $f^T = 81$ frames, setting the stride L to $\{3, 9, 27\}$ yields corresponding sparse sequence lengths of $f^S = \{27, 9, 3\}$ for the student network. This approach drastically lowers the computational cost for the student network while maintaining

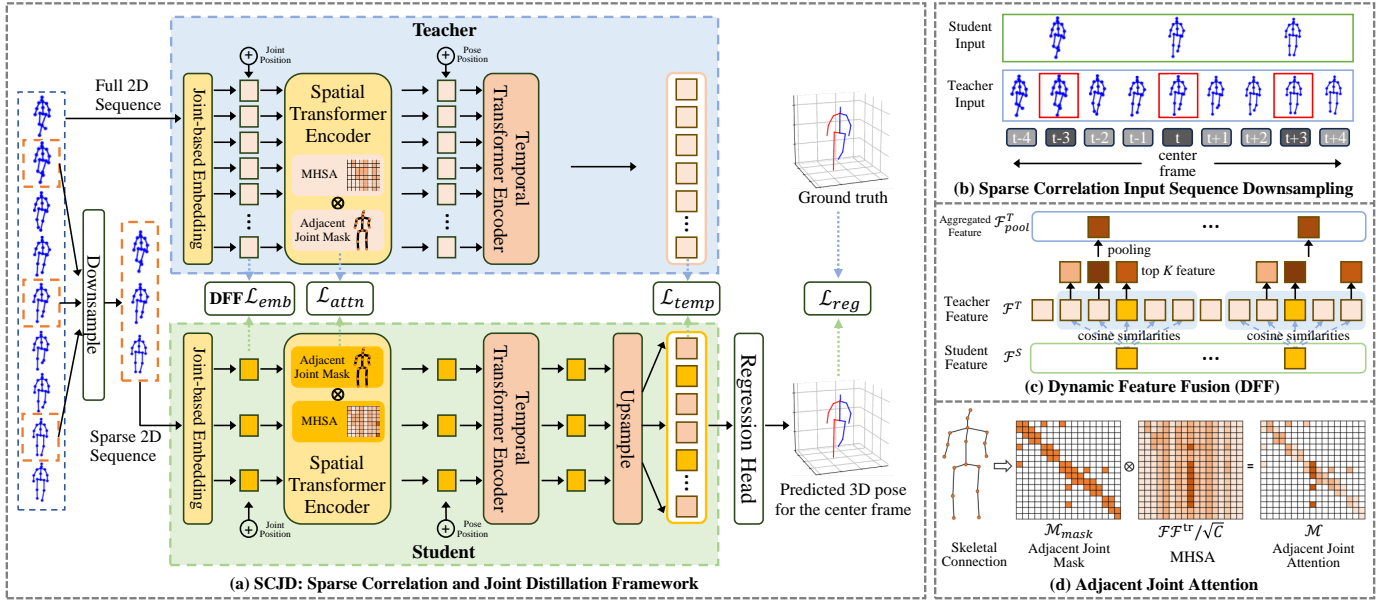


Fig. 2. Overview of the SCJD framework: SCJD comprises two transformer encoders that separately learn spatial and temporal information. The student model first employs *Sparse Correlation Input Sequence Downsampling* to reduce input redundancy while preserving temporal correlations. Then, through *Dynamic Joint Embedding Distillation* and *Adjacent Joint Attention Distillation*, knowledge from the teacher network’s spatial encoder is transferred to help the student model learn joint associations. Finally, *Temporal Consistency Distillation* facilitates the transfer of temporal knowledge from the teacher’s temporal encoder, enabling the student model to capture the temporal relationships between multi-frame postures.

the same large receptive field as the teacher network, ensuring an effective balance between efficiency and performance.

C. Dynamic Joint Spatial Attention Distillation

To capture the spatial relationships between human joints, we first utilize a spatial transformer to model the positional connections among joints in a frame of pose. For preprocessing the 2D pose sequence as network input, joint coordinates are linearly projected into a higher-dimensional space, and a learnable spatial positional embedding is added to encode the positions of the joints. Consequently, the joint embedding for each frame in the student and teacher networks are represented as $\mathcal{F}^S \in \mathbb{R}^{1 \times J \times C^S}$ and $\mathcal{F}^T \in \mathbb{R}^{1 \times J \times C^T}$, respectively, where C^S and C^T denote the feature dimensions of the joint-based embeddings. These features are then passed through a spatial transformer encoder. To minimize the model size, the student network utilizes a reduced feature dimension (C^S) compared to the teacher network (C^T).

Dynamic Joint Embedding Distillation. Our framework employs a sequence-to-frame approach, utilizing multi-frame 2D pose inputs to predict the 3D human pose of the central frame. To reduce computation, we apply sparse correlation input downsampling, which retains some degree of correlation while inevitably losing certain useful information due to the downsampling process. To address this limitation, we introduce a dynamic feature fusion (DFF) strategy, allowing the student network to learn multi-frame joint embedding features from the teacher network and improve its representation.

Specifically, in the early training stages (first N epochs), when the student network has not yet learned meaningful knowledge, we simply use evenly spaced intervals to align the

teacher sequence with the student’s downsampling sequence. In later stages, as the student begins to acquire knowledge from the teacher, we leverage the multi-frame features of the teacher to help the student emulate the teacher’s contextual feature. As shown in Fig. 2(c), for each pose p in the student network’s sampled sequence, we locate the corresponding pose p in the teacher network’s sequence. Centered at p , we extract a feature sequence $\{\mathcal{F}_k^T | k \in [p - (L - 1), p + (L - 1)]\}$ based on a predefined stride L . We then compute cosine similarities between each teacher feature \mathcal{F}_k^T and the student feature \mathcal{F}_p^S . The top- K teacher features with the highest similarity are pooled, producing \mathcal{F}_{pool}^T . Finally, we minimize the distance between \mathcal{F}_{pool}^T and \mathcal{F}_p^S , enabling the student to learn the teacher’s contextual relationships effectively. For the above two stages, the distillation loss of the joint-based embedding feature can be formulated as:

$$\mathcal{L}_{emb} = \begin{cases} \frac{1}{J} \sum_{i=1}^J \|\text{FC}(\mathcal{F}_{p,i}^S) - \mathcal{F}_{p,i}^T\|_2, & \text{epoch} \leq N, \\ \frac{1}{J} \sum_{i=1}^J \|\text{FC}(\mathcal{F}_{p,i}^S) - \mathcal{F}_{pool,i}^T\|_2, & \text{epoch} > N, \end{cases} \quad (1)$$

where $\text{FC}(\cdot)$ is a linear layer to align the joint-based embedding dimensions of the student’s C^S and the teacher’s C^T . Through dynamic joint embedding distillation, the student network can learn more effective context representations.

Adjacent Joint Attention Distillation. After aligning the joint embedding feature between the teacher and student networks, we initiate knowledge transfer from the teacher to the student. However, simply replicating the teacher network’s feature extraction capabilities makes it difficult for the student network to grasp the underlying relationships between human joints. Note that human posture is inherently represented as a skeletal model, where interconnected joints are linked by

bones, forming a robust prior topological structure, as shown in Fig. 2(d). Adjacent joints are defined as pairs of keypoints directly connected within this structure, thereby capturing the local spatial relationships of the human pose. The interactions between adjacent joints not only encode essential structural characteristics of the skeleton but also provide valuable spatial-temporal constraints and biomechanical priors for the model. These connectivities between adjacent joints are crucial prior knowledge that guides the student network to focus on these relationships, thereby enhancing its fundamental understanding of human posture. To incorporate this structural prior, we design an adjacent joint mask \mathcal{M}_{mask} , which enforces the student network to learn the teacher network’s multi-head self-attention (MHSA) patterns specifically between adjacent joints. This \mathcal{M}_{mask} can be expressed as:

$$\mathcal{M}_{mask}(i, j) = \begin{cases} 1, & \text{if bone } i \text{ is connected to bone } j, \\ 0, & \text{otherwise.} \end{cases} \quad (2)$$

To encourage the student network to focus on adjacent joint features derived from the teacher network, we multiply \mathcal{M}_{mask} with the MHSA matrix generated by both teacher and student network’s spatial encoder. This results in the adjacent joint attention \mathcal{M} , which filters out irrelevant elements in the attention matrix. The computation is expressed as:

$$\mathcal{M}(\mathcal{F}) = \frac{\mathcal{F}\mathcal{F}^{tr}}{\sqrt{C}} \otimes \mathcal{M}_{mask}, \quad (3)$$

where $\mathcal{F} \in \mathbb{R}^{J \times C}$ represents the features from the spatial encoder of either the student or teacher network, J is the total number of joints, C is the embedding dimension, and \mathcal{F}^{tr} denotes the transpose of the feature matrix. To align skeletal relationships, we propose an adjacent joint attention distillation method that minimizes the difference between the skeleton correlation matrices of the teacher and student networks. This is formulated as:

$$\mathcal{L}_{attn} = \sum_{i=1}^J \sum_{j=1}^J \|\mathcal{M}_{i,j}(\mathcal{F}^S) - \mathcal{M}_{i,j}(\mathcal{F}^T)\|_2. \quad (4)$$

This loss function encourages the student spatial encoder to better capture the relationships between adjacent joints, thereby improving its ability to understand the underlying skeletal structure for 3D human pose estimation.

D. Temporal Consistency Distillation

To enhance the smoothness of 3D HPE predictions across consecutive frames, we further process the temporal relationships between frames after capturing the spatial relationships between joints. For input sequences of lengths f^T (teacher) and f^S (student), the output features from their respective spatial transformer encoders are represented as $Z^T \in \mathbb{R}^{f^T \times (J \cdot C^T)}$ and $Z^S \in \mathbb{R}^{f^S \times (J \cdot C^S)}$. To retain frame temporal position information, a learnable temporal positional embedding is added to Z^T and Z^S . These features, enriched with temporal positional embeddings, are then passed through their respective temporal transformer encoders to capture frame-to-frame dependencies across the sequence. The outputs are denoted as

$Y^T \in \mathbb{R}^{f^T \times (J \cdot C^T)}$ and $Y^S \in \mathbb{R}^{f^S \times (J \cdot C^S)}$, corresponding to the teacher and student networks, respectively.

To generate dense 3D poses for all frames within the receptive field, we upsample the student network’s final-layer features using a 1D deconvolution operation f_{deconv} to match the frame length of the teacher network. A fully connected layer is then applied to align the feature dimensions C^S and C^T . The recovered sequence is expressed as:

$$\hat{Y}^S = \text{FC}(f_{deconv}(Y^S)), \quad (5)$$

where $\hat{Y}^S \in \mathbb{R}^{f^T \times (J \cdot C^T)}$. This step enables the transfer of comprehensive information from the teacher network’s receptive field to the student network via token-level feature distillation. The temporal distillation process is formulated as:

$$\mathcal{L}_{temp} = \frac{1}{f^T} \sum_{i=1}^{f^T} \|\hat{Y}_i^S - Y_i^T\|_2. \quad (6)$$

To further enhance prediction accuracy, we employ the Mean Per Joint Position Error (MPJPE) loss [27] to regress the error between the predicted results and the ground truth. Since the recovered sequence $\hat{Y}^S \in \mathbb{R}^{f^T \times (J \cdot C^T)}$ is used to predict the 3D pose of the central frame, we apply a 1D convolution to aggregate temporal information, producing an output $\hat{y} \in \mathbb{R}^{1 \times (J \cdot C^T)}$. This output is then passed through a linear projection to map \hat{y} into the pose representation $\hat{y} \in \mathbb{R}^{1 \times (J \cdot 3)}$. The regression loss can be expressed as:

$$\mathcal{L}_{reg} = \frac{1}{J} \sum_{i=1}^J \|\hat{y}_i - y_i\|_2, \quad (7)$$

where \hat{y}_i and y_i represent the predicted 3D joint position and the ground truth respectively.

Thus, the total loss \mathcal{L}_{total} of our proposed SCJD is:

$$\mathcal{L}_{total} = \mathcal{L}_{reg} + \alpha \mathcal{L}_{emb} + \beta \mathcal{L}_{attn} + \gamma \mathcal{L}_{temp}, \quad (8)$$

where α , β , and γ are the weights of each component of the loss, respectively.

IV. EXPERIMENTS

A. Experimental Settings

Datasets and Metrics. We evaluated our model on two datasets, namely Human3.6M [27] and MPI-INF-3DHP [28]. For Human3.6M [27], we compute Mean Per Joint Position Error (MPJPE), which is the average euclidean distance in millimeters between the predicted and the ground-truth 3D joint coordinates. To evaluate the efficiency, we use Floating-Point operations (FLOPs) to measure the computational cost. For MPI-INF-3DHP [28], we additionally compute the Percentage of Correct Keypoints (PCK) within a range of 150 mm, and Area Under Curve (AUC) for a range of PCK thresholds.

Implementation Details. The input sequence lengths of the student network are $f^S = \{3, 9, 27\}$. For the teacher network, we chose $f^T = 81$. The embedding dimensions of the student and teacher network are $C^S = 16$ and $C^T = 32$. The number of joints $J = 17$. In dynamic token matching, we set $N = 20$, $K = 3$. We empirically set the hyperparameters of Eq. 8 to $\alpha = \beta = 1$, $\gamma = 0.01$. We trained our model for 50

TABLE I
COMPARISONS WITH PREVIOUS METHODS ON HUMAN3.6M. THE 2D
POSES OBTAINED BY CPN [29] ARE USED AS INPUTS. BEST IN RED,
SECOND BEST IN BLUE.

Method	Publication	f	Params(M)	MFLOPs↓	MPJPE↓
MoVNect [18]	WACV'20	1	1.03	1.35	97.3
MobileHuman [21]	CVPRW'21	1	2.24	3920	56.9
PoseFormer [26]	ICCV'21	3	9.58	60.4	51.8
UAU [30]	WACV'23	3	10.36	535	49.9
MixSTE [9]	CVPR'22	3	33.70	3420	49.6
MHFormer [10]	CVPR'22	3	18.92	114.4	48.7
HDFormer [8]	IJCAI'23	3	3.70	163	48.7
STCFormer [7]	CVPR'23	3	4.75	484.1	48.5
KTPFormer [6]	CVPR'24	3	34.73	3540	47.3
RePOSE [5]	ECCV'24	3	15.94	1618.4	47.3
PoseFormerV2 [15]	CVPR'23	3	14.36	117.3	47.1
SCJD (Ours)		3	2.79	51.2	47.0
PoseFormer [26]	ICCV'21	9	9.58	150	49.9
PAA [11]	TIP'22	9	6.21	1139.1	48.9
UAU [30]	WACV'23	9	10.36	543	47.9
MHFormer [10]	CVPR'22	9	18.92	342.9	47.8
HDFormer [8]	IJCAI'23	9	3.70	367.2	47.3
KTPFormer [6]	CVPR'24	9	34.74	10610	46.6
RePOSE [5]	ECCV'24	9	15.94	4860	46.5
PoseFormerV2 [15]	CVPR'23	9	14.36	351.7	46.0
SCJD (Ours)		9	2.79	81.3	46.3
UAU [30]	WACV'23	27	10.36	564	47.4
PoseFormer [26]	ICCV'21	27	9.59	452	47.0
PAA [11]	TIP'22	27	6.21	1229.5	46.8
MHFormer [10]	CVPR'22	27	18.92	1031.8	45.9
HDFormer [8]	IJCAI'23	27	3.70	652.2	45.8
KTPFormer [6]	CVPR'24	27	34.77	31840	45.4
PoseFormerV2 [15]	CVPR'23	27	14.36	1054.8	45.2
RePOSE [5]	ECCV'24	27	15.95	14560	44.1
SCJD (Ours)		27	2.80	171.5	45.2

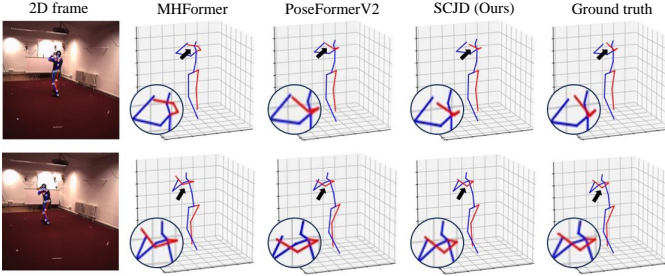


Fig. 3. Comparison of visualization results between ours and MHFormer [10] and PoseFormerV2 [15] on Human3.6M test set S11 with the *Photo* action. The black arrows highlight locations where our method has better results.

epochs using the Adam optimizer with learning rate of $1e-3$ and weight decay of 0.1. For the network structure and other more details, please refer to the supplementary material.

B. Comparisons with State-of-the-art Methods

We quantitatively compare our student network's result with previous 3D HPE methods on Human3.6M [27], as shown in Table I, where f denotes the input sequence's length. For each f , we have achieved the minimum number of parameters, the minimum computational cost, and the optimal or suboptimal accuracy. Notably, when f is 27, with the same accuracy as PoseformerV2 [15], we have improved the speed by 6.15 times. When f is 3, with the similar computational cost to PoseFormer [26], we have improved the accuracy by 4.8mm MPJPE. Compared with the single-frame input methods [18],

TABLE II
COMPARISONS WITH PREVIOUS LOW-FRAME-RATE METHODS ON
MPI-INF-3DHP. USING GROUND-TRUTH 2D POSES AS INPUTS. BEST IN
RED, SECOND BEST IN BLUE.

Method	Publication	f	MFLOPs↓	PCK↑	AUC↑	MPJPE↓
PoseFormer [26]	ICCV'21	9	150	88.6	56.4	77.1
CrossFormer [31]	arXiv'22	9	163	89.1	57.5	76.3
PAA [11]	TIP'22	9	1139.1	90.3	57.8	69.4
MHFormer [10]	CVPR'22	9	342.9	93.8	63.3	58.0
UAU [30]	WACV'23	9	543	95.4	67.6	46.9
DualFormer [32]	TCSVT'24	9	-	97.8	73.4	40.1
STCFormer [7]	CVPR'23	9	484.1	98.2	81.5	28.2
SCJD (Ours)		9	81.3	97.5	76.5	30.7
SCJD (Ours)		27	171.5	98.4	79.1	27.0

TABLE III
COMPARISONS WITH TRADITIONAL KD METHODS ON HUMAN3.6M.
THE 2D POSES OBTAINED BY CPN [29] ARE USED AS INPUTS. BEST IN
RED, SECOND BEST IN BLUE.

Method	Publication	f	MFLOPs↓	MPJPE↓
SP [33]	ICCV'19	81	406.2	49.8
DKD [34]	CVPR'22	81	406.2	49.3
PKT [35]	ECCV'18	81	406.2	48.8
SimKD [36]	CVPR'22	81	406.2	47.9
KDSVD [37]	ECCV'18	81	406.2	47.7
RKD [38]	CVPR'19	81	406.2	46.8
SCJD (Ours)		27	171.5	45.2

[21], our SCJD significantly improves the accuracy, which proves that multi-frame input can effectively alleviate the ambiguity of 3D HPE. Our SCJD is the only one that balances computational cost and accuracy. It proves that the student network benefits from sparse input, which significantly reduces the computational cost, and multiple distillations improve its accuracy. The visual comparisons are shown in Fig. 3, compared with MHFormer [10] and PoseFormerV2 [15], our SCJD achieves more accurate gesture positions and joint position relationships thanks to the skeleton-prior distillation.

We also evaluate our method on MPI-INF-3DHP [28]. As shown in Table II, with the same fewer input sequences, our method can best achieve a balance between accuracy and complexity, which proves the effectiveness of our SCJD.

C. Comparisons with Knowledge Distillation Methods

As shown in Table III, we re-implemented the general knowledge distillation method and demonstrated that SCJD achieves higher accuracy than other distillation approaches, even with smaller input sequences and lower computational requirements. Unlike traditional knowledge distillation methods, SCJD enables the student network to effectively learn both the spatial dependencies between joints within a pose and the temporal dependencies between frames in a sequence. This is achieved through our carefully designed *Dynamic Joint Spatial Attention Distillation* and *Temporal Consistency Distillation*, resulting in significantly improved accuracy.

D. Ablation Study

Impact of Different Parts. In Table IV, we investigate the impact of sequence downsampling and distillation on the student network. RF represents the Receptive Field, which

TABLE IV
ABLATION STUDY ON DIFFERENT PARTS ON HUMAN3.6M

Sampling	Distillation	f	RF	Params(M)	MFLOPs↓	MPJPE↓
✗	✗	27	27	2.41	135.4	51.4
✓	✗	27	81	2.80	171.5	48.9
✗	✗	81	81	2.43	406.2	48.5
✗	✓	81	81	2.43	406.2	46.1
✓	✓	27	81	2.80	171.5	45.2

TABLE V
ABLATION STUDY ON DISTILLATION COMPONENTS ON HUMAN3.6M

Method	f	\mathcal{L}_{reg}	\mathcal{L}_{emb}	\mathcal{L}_{am}	\mathcal{L}_{temp}	MPJPE↓
w/o \mathcal{L}_{emd}	27	✓	✗	✓	✓	46.5
w/o \mathcal{L}_{attn}	27	✓	✓	✗	✓	48.2
w/o \mathcal{L}_{temp}	27	✓	✓	✓	✗	47.3
full	27	✓	✓	✓	✓	45.2

TABLE VI
ABLATION STUDY ON PARAMETER SETTINGS ON HUMAN3.6M

Model	f	C	L	Params(M)	MFLOPs↓	MPJPE↓
Teacher	81	32	4	9.60	1358	44.3
	27	16	4	2.80	171.5	45.2
	9	16	4	2.79	81.3	46.3
Student	27	8	4	0.71	42.6	47.5
	9	8	4	0.71	20.1	47.8
	27	16	2	1.60	104.2	46.8
	9	16	2	1.60	58.8	47.2

is the length of the sequence before sampling. From Rows 1 and 2, sequence downsampling brings an improvement of 2.5mm MPJPE. We can think that the sparse sequence obtained by sampling is equivalent to expanding the receptive field under the same input length. From Rows 3 and 4, distillation improves the accuracy by 2.4mm MPJPE, which proves the effectiveness of knowledge transfer. The last row shows that performance is optimal when all modules are included. Compared with the same 27-frame input (Row 1), the performance is significantly improved by 6.2mm MPJPE.

Impact of Distillation Components. In Table V, we investigate the impact of various distillation components on the student model. Table V shows that any of the three distillations plays an important role because they all convey corresponding knowledge. Besides, we can find that the impact of \mathcal{L}_{am} is particularly obvious, which proves that attention distillation combined with skeletal priors better learns joint relationships.

The Smaller Model. In Table VI, we compared the performance of the student and the teacher model. The student model achieves an acceptable loss of accuracy in exchange for significantly fewer Params and FLOPs. To further reduce the student model’s size, we respectively reduce the feature dimensions of the joint-based embeddings C and the number of layers L in both spatial and temporal transformers. From Rows 4 and 5, we observed that further reducing the embedding dimension reduces the computational cost and maintains respectable accuracy, suggesting that reducing the embedding dimension also preserves feature representation capabilities via distillation. Notably, in Row 5, when f is 9, 47.8mm MPJPE can be achieved with only 20.1 MFLOPs, which is comparable to the accuracy of MHFormer [10], but we are about 17.0 times

TABLE VII
ABLATION STUDY ON PARAMETER SETTING OF LOSS FUNCTION.

α	β	γ	MPJPE↓
1	1	0.01	45.2
1	1	0.1	45.3
1	1	1	45.3
0.01	0.01	1	45.7
0.1	0.1	1	45.5

faster than it. From Rows 6 and 7, reducing depth degrades accuracy, because too few layers will weaken the ability to extract more complex features at different layers.

Hyperparameter Analysis. We have further analyzed the hyperparameters of the loss function (Eq. 8), with the corresponding results summarized in Table VII. Specifically, we examine the weights α , β , and γ , which correspond to the individual loss components. The results indicate that our method achieves the best performance when $\alpha = \beta = 1$ and $\gamma = 0.01$. We attribute this to the fact that these settings effectively scale the losses to the same order of magnitude, thereby facilitating more stable and balanced optimization. We will add this analysis and discussion in the revision.

V. CONCLUSION

This paper proposes SCJD, effectively addresses the limitations of existing 3D HPE methods by combining sparse correlation input sequence downsampling with advanced dynamic joint spatial attention distillation techniques. By preserving inter-frame correlations, enhancing spatial understanding, and aligning temporal consistency, SCJD significantly reduces computational overhead while maintaining high accuracy. Extensive experiments validate its superior performance, making SCJD a promising solution for efficient and accurate 3D HPE.

REFERENCES

- [1] Jathushan Rajasegaran, Georgios Pavlakos, Angjoo Kanazawa, Christoph Feichtenhofer, and Jitendra Malik, “On the benefits of 3d pose and tracking for human action recognition,” in *CVPR*, 2023, pp. 640–649.
- [2] Lilang Lin, Jiahang Zhang, and Jiaying Liu, “Mutual information driven equivariant contrastive learning for 3d action representation learning,” *IEEE TIP*, vol. 33, pp. 1883–1897, 2024.
- [3] Hua Yu, Xuanzhe Fan, Yaqing Hou, Wenbin Pei, Hongwei Ge, Xin Yang, Dongsheng Zhou, Qiang Zhang, and Mengjie Zhang, “Toward realistic 3d human motion prediction with a spatio-temporal cross-transformer approach,” *IEEE TCSVT*, vol. 33, no. 10, pp. 5707–5720, 2023.
- [4] Peng Xiao, Yi Xie, Xuemiao Xu, Weihong Chen, and Huaidong Zhang, “Multi-person pose forecasting with individual interaction perceptron and prior learning,” in *ECCV*, 2024, pp. 402–419.
- [5] Ziming Sun, Yuan Liang, Zejun Ma, Tianle Zhang, Linchao Bao, Guiqing Li, and Shengfeng He, “Repose: 3d human pose estimation via spatio-temporal depth relational consistency,” in *ECCV*, 2024.
- [6] Jihua Peng, Yanghong Zhou, and P. Y. Mok, “Ktpformer: Kinematics and trajectory prior knowledge-enhanced transformer for 3d human pose estimation,” in *CVPR*, 2024, pp. 1123–1132.
- [7] Zhenhua Tang, Zhaofan Qiu, Yanbin Hao, Richang Hong, and Ting Yao, “3d human pose estimation with spatio-temporal criss-cross attention,” in *CVPR*, 2023, pp. 4790–4799.
- [8] Hanyuan Chen, Jun-Yan He, Wangmeng Xiang, Zhi-Qi Cheng, Wei Liu, Hanbing Liu, Bin Luo, Yifeng Geng, and Xuansong Xie, “Hdformer: high-order directed transformer for 3d human pose estimation,” in *IJCAI*, 2023.

- [9] Jinlu Zhang, Zhigang Tu, Jianyu Yang, Yujin Chen, and Junsong Yuan, "Mixste: Seq2seq mixed spatio-temporal encoder for 3d human pose estimation in video," in *CVPR*, 2022, pp. 13232–13242.
- [10] Wenhao Li, Hong Liu, Hao Tang, Pichao Wang, and Luc Van Gool, "Mhformer: Multi-hypothesis transformer for 3d human pose estimation," in *CVPR*, 2022, pp. 13147–13156.
- [11] Youze Xue, Jiansheng Chen, Xiangming Gu, Huimin Ma, and Hongbing Ma, "Boosting monocular 3d human pose estimation with part aware attention," *IEEE TIP*, vol. 31, pp. 4278–4291, 2022.
- [12] Zikai Huang, Xuemiao Xu, Cheng Xu, Huaidong Zhang, Chenxi Zheng, Jing Qin, and Shengfeng He, "Beat-it: Beat-synchronized multi-condition 3d dance generation," in *ECCV*. Springer, 2024, pp. 273–290.
- [13] Alexey Dosovitskiy, Lucas Beyer, Alexander Kolesnikov, Dirk Weissenborn, Xiaohua Zhai, Thomas Unterthiner, Mostafa Dehghani, Matthias Minderer, Georg Heigold, Sylvain Gelly, Jakob Uszkoreit, and Neil Houlsby, "An image is worth 16x16 words: Transformers for image recognition at scale," in *ICLR*, 2021.
- [14] Wenhao Li, Hong Liu, Runwei Ding, Mengyuan Liu, Pichao Wang, and Wenming Yang, "Exploiting temporal contexts with strided transformer for 3d human pose estimation," *IEEE TMM*, vol. 25, pp. 1282–1293, 2022.
- [15] Qitao Zhao, Ce Zheng, Mengyuan Liu, Pichao Wang, and Chen Chen, "Poseformerv2: Exploring frequency domain for efficient and robust 3d human pose estimation," in *CVPR*, 2023, pp. 8877–8886.
- [16] Zhenhua Tang, Yanbin Hao, Jia Li, and Richang Hong, "Ftcm: Frequency-temporal collaborative module for efficient 3d human pose estimation in video," *IEEE TCSVT*, vol. 34, no. 2, pp. 911–923, 2024.
- [17] Geoffrey Hinton, Oriol Vinyals, and Jeff Dean, "Distilling the knowledge in a neural network," *arXiv preprint arXiv:1503.02531*, 2015.
- [18] Dong-Hyun Hwang, Suntae Kim, Nicolas Monet, Hideki Koike, and Soonmin Bae, "Lightweight 3d human pose estimation network training using teacher-student learning," in *WACV*, 2020, pp. 479–488.
- [19] Dong-hwi Kim, Dong-hun Lee, Aro Kim, Jinwoo Jeong, Jong Taek Lee, Sungjei Kim, and Sang-hyo Park, "Pruning-guided feature distillation for an efficient transformer-based pose estimation model," *IET Computer Vision*, vol. 18, no. 6, pp. 745–758, 2024.
- [20] Cunling Bian, Weigang Lu, Feng Wei, and Song Wang, "Learning with privileged stereo knowledge for monocular absolute 3d human pose estimation," *Available at SSRN*, 2024.
- [21] Sangbum Choi, Seokeon Choi, and Changick Kim, "Mobilehumanpose: Toward real-time 3d human pose estimation in mobile devices," in *CVPR Workshops*, 2021, pp. 2328–2338.
- [22] Bangzhen Liu, Yangyang Xu, Cheng Xu, Xuemiao Xu, and Shengfeng He, "Open-set mixed domain adaptation via visual-linguistic focal evolving," *IEEE TCSVT*, , no. 99, pp. 1–1, 2025.
- [23] Haoxin Yang, Xuemiao Xu, Cheng Xu, Huaidong Zhang, Jing Qin, Yi Wang, Pheng-Ann Heng, and Shengfeng He, "G 2 face: High-fidelity reversible face anonymization via generative and geometric priors," *IEEE TIFS*, 2024.
- [24] Bangzhen Liu, Chenxi Zheng, Xuemiao Xu, Cheng Xu, Huaidong Zhang, and Shengfeng He, "Rotation-adaptive point cloud domain generalization via intricate orientation learning," *IEEE TPAMI*, 2025.
- [25] Peng Xiao, Chuang Wang, Ze Lin, Ying Hao, Gang Chen, and Longhan Xie, "Knowledge-based clustering federated learning for fault diagnosis in robotic assembly," *Knowledge-Based Systems*, vol. 294, pp. 111792, 2024.
- [26] Ce Zheng, Sijie Zhu, Matias Mendieta, Taojiannan Yang, Chen Chen, and Zhengming Ding, "3d human pose estimation with spatial and temporal transformers," in *ICCV*, 2021, pp. 11656–11665.
- [27] Catalin Ionescu, Dragos Papava, Vlad Olaru, and Cristian Sminchisescu, "Human3.6m: Large scale datasets and predictive methods for 3d human sensing in natural environments," *IEEE TPAMI*, vol. 36, no. 7, pp. 1325–1339, 2013.
- [28] Dushyant Mehta, Helge Rhodin, Dan Casas, Pascal Fua, Oleksandr Sotnychenko, Weipeng Xu, and Christian Theobalt, "Monocular 3d human pose estimation in the wild using improved cnn supervision," in *3DV*, 2017, pp. 506–516.
- [29] Yilun Chen, Zhicheng Wang, Yuxiang Peng, Zhiqiang Zhang, Gang Yu, and Jian Sun, "Cascaded pyramid network for multi-person pose estimation," in *CVPR*, 2018, pp. 7103–7112.
- [30] Moritz Einfalt, Katja Ludwig, and Rainer Lienhart, "Uplift and upsample: Efficient 3d human pose estimation with uplifting transformers," in *WACV*, 2023, pp. 2903–2913.
- [31] Mohammed Hassanin, Abdelwahed Khamiss, Mohammed Bennamoun, Farid Boussaid, and Ibrahim Radwan, "Crossformer: Cross spatio-temporal transformer for 3d human pose estimation," *arXiv preprint arXiv:2203.13387*, 2022.
- [32] Lu Zhou, Yingying Chen, and Jinqiao Wang, "Dual-path transformer for 3d human pose estimation," *IEEE TCSVT*, vol. 34, no. 5, pp. 3260–3270, 2024.
- [33] Frederick Tung and Greg Mori, "Similarity-preserving knowledge distillation," in *ICCV*, 2019, pp. 1365–1374.
- [34] Borui Zhao, Quan Cui, Renjie Song, Yiyu Qiu, and Jiajun Liang, "Decoupled knowledge distillation," in *CVPR*, 2022, pp. 11953–11962.
- [35] Nikolaos Passalis and Anastasios Tefas, "Learning deep representations with probabilistic knowledge transfer," in *ECCV*, 2018, pp. 268–284.
- [36] Defang Chen, Jian-Ping Mei, Hailin Zhang, Can Wang, Yan Feng, and Chun Chen, "Knowledge distillation with the reused teacher classifier," in *CVPR*, 2022, pp. 11933–11942.
- [37] Seung Hyun Lee, Dae Ha Kim, and Byung Cheol Song, "Self-supervised knowledge distillation using singular value decomposition," in *ECCV*, 2018, pp. 335–350.
- [38] Wonpyo Park, Dongju Kim, Yan Lu, and Minsu Cho, "Relational knowledge distillation," in *CVPR*, 2019, pp. 3967–3976.
- [39] Ashish Vaswani, Noam Shazeer, Niki Parmar, Jakob Uszkoreit, Llion Jones, Aidan N. Gomez, Łukasz Kaiser, and Illia Polosukhin, "Attention is all you need," in *NeurIPS*, 2017, p. 6000–6010.
- [40] Ke Sun, Bin Xiao, Dong Liu, and Jingdong Wang, "Deep high-resolution representation learning for human pose estimation," in *CVPR*, 2019, pp. 5686–5696.
- [41] Dario Pavlo, Christoph Feichtenhofer, David Grangier, and Michael Auli, "3d human pose estimation in video with temporal convolutions and semi-supervised training," in *CVPR*, 2019, pp. 7753–7762.
- [42] Diederik P Kingma and Jimmy Ba, "Adam: A method for stochastic optimization," *arXiv preprint arXiv:1412.6980*, 2014.

Supplementary Material

The supplementary material contains: 1) Additional Details of the Network Structure; 2) More Experimental Details; 3) Qualitative Comparisons on In-the-wild Videos; 4) More Qualitative Comparisons on Human3.6M.

VI. ADDITIONAL DETAILS OF THE NETWORK STRUCTURE

In our framework, spatial transformers, as shown in Fig. 4(a), are used to model the positional connections among joints in a frame of pose. Building on PoseFormer [26], for each frame of the input 2D pose sequence, coordinates of all joints of a pose are linearly projected to a higher-dimensional space, and a learnable spatial positional embedding is added to encode the positions of the joints. These features are then passed through a spatial transformer encoder. Then, the output of each frame of the spatial transformer encoder is concatenated as the input of the temporal transformer encoder, as shown in Fig. 4(b). Temporal transformer encoders capture frame-to-frame dependencies across the sequence, and its output is passed through the regression head to obtain the 3D pose for the center frame.

The spatial transformer encoder and temporal transformer encoder in our framework both adopt the standard transformer encoder architecture [39], as illustrated in Fig. 4(c). This architecture consists of N identical layers, each comprising two main components: a Multi-Head Self-Attention (MHSA) mechanism and a Feed Forward Network (FFN). Layer Normalization (Layer Norm) is applied before the MHSA and FFN to stabilize training, while residual connections are employed around these sublayers to improve gradient flow and facilitate efficient learning. The MHSA module enables the encoder to capture complex dependencies within the input sequences, while the FFN refines the intermediate representations.

VII. MORE EXPERIMENTAL DETAILS

The datasets used in our experiment are Human3.6M [27] and MPI-INF-3DHP [28], which are the most widely used in 3D human pose estimation.

Human3.6M is the most widely used public indoor dataset for 3D human pose estimation. Eleven professional actors performed 15 actions including sitting, walking, discussing, photoing, sitting down, etc. Human3.6M consists of 3.6 million video frames with 3D ground truth annotations captured by a precise marker-based motion capture system. We adopt the same experimental setup as the previous work [5]–[7], [9], [10]: the model is trained on five sections (Subjects S1, S5, S6, S7, S8), and tested on two sections (Subjects S9 and S11). In common with existing 2D to 3D lifting work, we use 2D poses from CPN [29] during student network training and evaluation.

MPI-INF-3DHP is smaller but more challenging than Human3.6M. In addition to indoor collection, it also collects data outdoors, containing different themes and actions. We use ground truth 2D poses in our experiments on MPI-INF-3DHP for comparison with existing work [7], [10], [11], [31], [32].

Evaluation Metrics. For Human3.6M, we use the most common evaluation metric Mean Per Joint Position Error

(MPJPE), the average euclidean distance in millimeters between the predicted and the ground-truth 3D joint coordinates, to evaluate our estimation performance. For MPI-INF-3DHP, we use MPJPE, Percent Correct Keypoints (PCK) within a range of 150 mm, and Area Under the Curve (AUC) with a threshold range of 5-150 mm. To evaluate the efficiency of the model, we use FLOating-Point operations (FLOPs) to measure the computational cost.

Implementation Details. The input sequence length of the teacher model is $f_T = 81$. For the student model, we chose three different frame sequence lengths, i.e., $f_S = 3$, $f_S = 9$, and $f_S = 27$. Pose level flipping was applied as a data augmentation in training and testing [41]. We trained our model using the Adam [42] optimizer for 50 epochs with a weight decay of 0.1. We adopt an exponential learning rate decay schedule with an initial learning rate of $1e-3$ and a decay factor of 0.98 for each epoch. An NVIDIA GeForce RTX 4090 GPU is used for training with the batch size set to 1024. The details about model parameters of teacher network and student network with results are discussed in the ablation studies (Sec. IV-C of the article: The Smaller Model).

VIII. QUALITATIVE COMPARISONS ON IN-THE-WILD VIDEOS

To further validate the generalization ability of our model, we collected some wild videos as additional real-world tests. In our videos, figure skating is a sport with large movements, complex postures, and fast speeds, especially with frequent occlusions between body joints. As shown in Fig. 5, our method shows excellent accuracy in most frames of the wild videos. The black arrows point out the locations where our method is significantly more accurate than the state-of-the-art efficient pose estimation method PoseFormerV2 [15]. Our results are especially better in fast-moving poses, which proves that the student network can learn richer contextual information from the teacher network. In addition, our joint position relationship is more reasonable, thanks to the adjacent joint attention distillation.

IX. MORE QUALITATIVE COMPARISONS ON HUMAN3.6M

In this section, we supplement and present more qualitative results of our SCJD. Photo, Sitting Down, and Walkdog are more challenging actions in the Human3.6M test set. Fig. 6 shows a visual comparison of 3D pose estimation results between our SCJD and the representative method MHFormer [10]. The black arrow highlights locations where we clearly has better results compared to MHFormer [10]. It can be intuitively seen that our SCJD achieves more accurate hand and leg posture positions and joint position relationships.

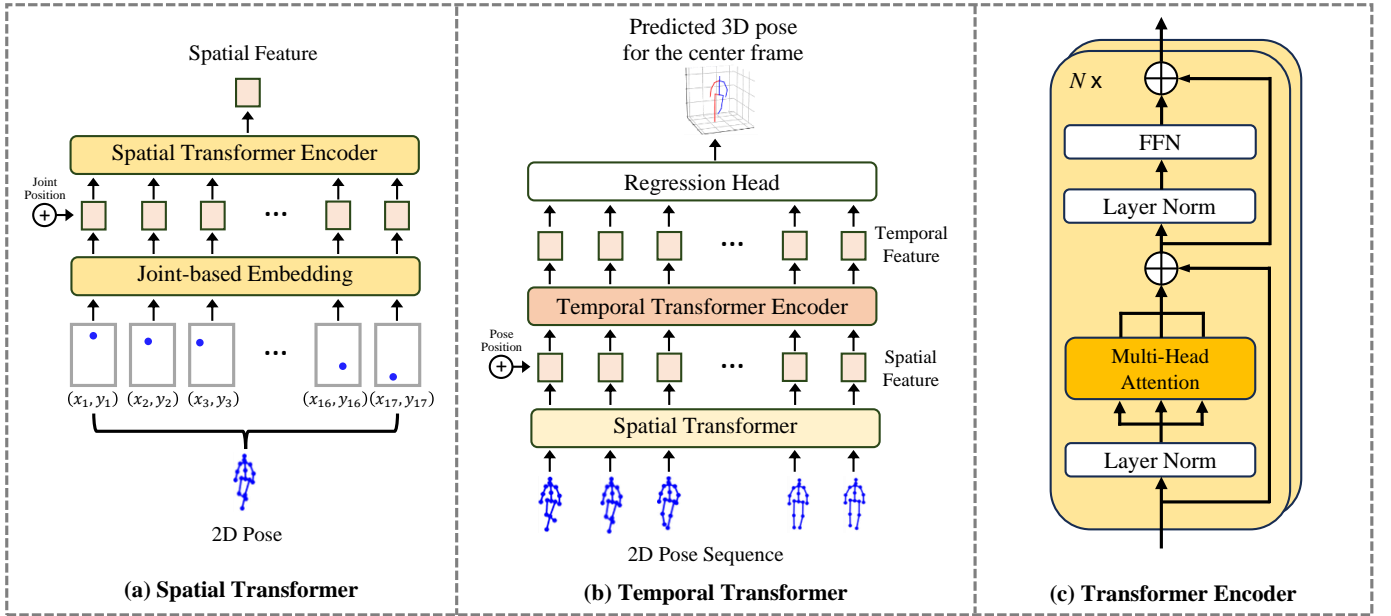


Fig. 4. Left: details of the spatial transformer. Center: details of the temporal transformer. Right: details of the transformer encoder structure.



Fig. 5. Qualitative comparisons between ours and PoseFormerV2 [15] on in-the-wild videos. The same visualization setting as PoseFormerV2 [15] is adopted, the 2D pose is obtained by the detector HRNet [40], and the number of input frames of the model is $f=27$. The black arrows highlight locations where our method clearly has better results.

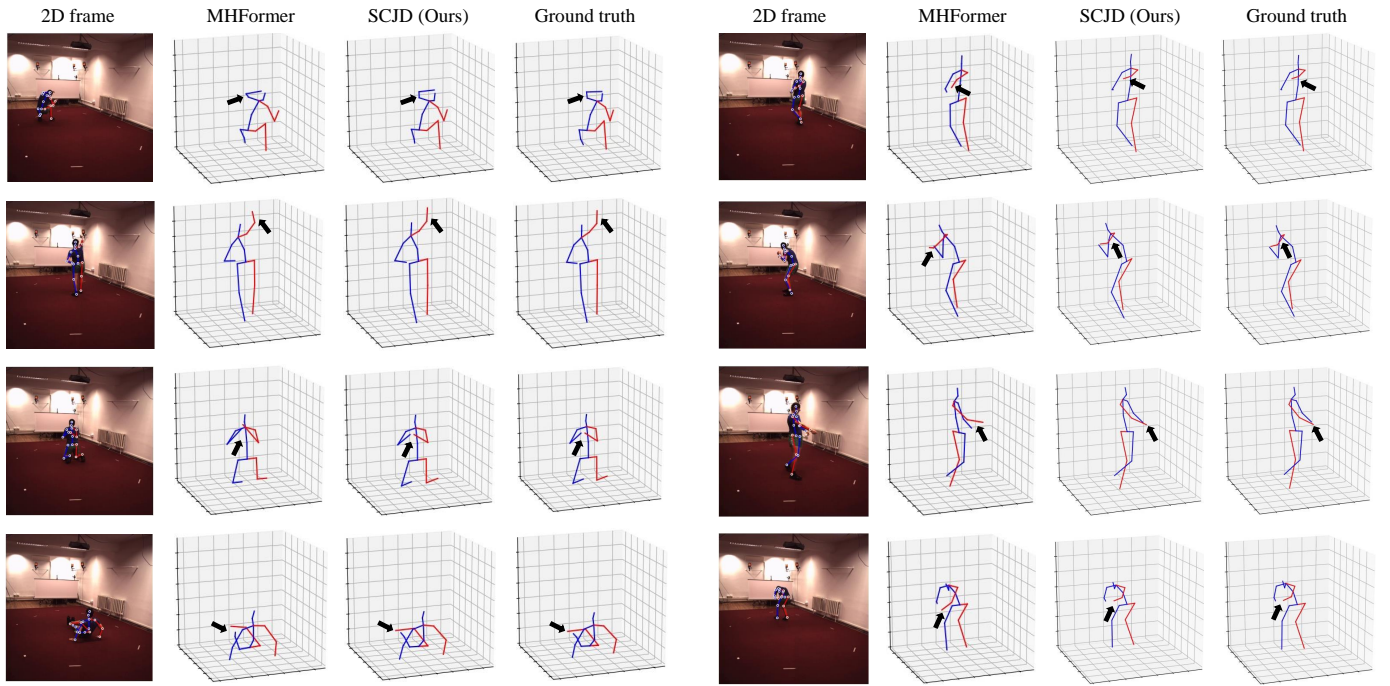


Fig. 6. Comparison of visualization results between ours and MHFormer [10] on Human3.6M test set S11 with the *Photo*, *Sitting Down*, and *Walkdog* actions. The 2D pose is obtained by the detector CPN [29], and the number of input frames of the model is $f=27$. The black arrows highlight locations where our method clearly has better results.